Check for updates

Manganese dioxide core–shell nanostructure to achieve excellent cycling stability for asymmetric supercapacitor applications

Quanbing Liu,[a] Juan Yang,[b] Rongfang Wang, (iD) *[b] Hui Wang[b] and Shan Ji*[ac]

This study presents a facile and low-cost method to prepare core–shell nano-structured β-MnO$_2$@δ-MnO$_2$, in which β-MnO$_2$ nano-wires act as the cores to form 3D networks and δ-MnO$_2$ as the shells. A uniform hierarchical β-MnO$_2$@δ-MnO$_2$ core–shell structure can be obtained after layered structured δ-MnO$_2$ is deposited on the surface of the needle-like β-MnO$_2$ particles *via* a simple wet chemistry method at room temperature. The as-prepared materials were physically and electrochemically characterized by nitrogen isotherm analysis, X-ray diffraction, scanning electron microscopy, transmission electron microscopy and potentiostatically/galvanostatically. Under our conditions, the electrochemical results showed that the specific capacitance of β-MnO$_2$@δ-MnO$_2$ was $\sim$200 F g^{-1} and the specific capacitance retention was almost 100% after 5000 cycles at a current density of 1 A g^{-1} in 1 M LiOH electrolyte. The excellent cycling stability of β-MnO$_2$@δ-MnO$_2$ showed that the new material has great potential for use in electrochemical supercapacitors, and the facile wet chemistry method used to synthesize β-MnO$_2$@δ-MnO$_2$ could be a promising method to produce highly stable MnO$_2$-based electrode materials in large batches.

1. Introduction

High-performance supercapacitors have received enormous interest as promising Energy Storage Devices (ESDs) for mobile electronics, backup power supplies and electric vehicles due to their high power density, fast charge/discharge capability and long cycle life.[1–4] Electrochemical supercapacitors using MnO$_2$ as electrode materials have attracted significant attention; this is due to the fact that they possess high theoretical capacitance, large electrode potential window, and are low-cost, non-toxic and environmentally benign in comparison to those using ruthenium oxides or other transition metal oxide electrodes.[5–8] MnO$_2$ of various crystallographic polymorphs (such as α-, β-, δ-, γ- and ε-MnO$_2$) consist of MnO$_6$ units in which each Mn^{4+} is surrounded by six oxygen atoms.[9] It was found that polymorphs consisting of MnO$_6$ octahedra are interlinked yielding various structures with different tunnels or interlayers.[10] Moreover, the charge storage in transition metal oxides is a multi-step process involving electrolyte ion transfer on the interface of the electrode/electrolyte and the intercalation/deintercalation of cations. Recent studies showed that materials possessing two-

dimensional (2D) layered structure and wide interlayer spacing are ideal electrode materials for electrochemical supercapacitors, providing promising features, *e.g.* favouring the transport of electrolyte ions and the intercalation/deintercalation processes, leading to highly efficient ESDs.[11]

The capacitance properties of MnO$_2$ strongly rely upon the intercalation/deintercalation of cations into or from its structure in aqueous electrolytes, indicating that structures with large size tunnels or interlayers result in better capacitance performance.[10] Among all these MnO$_2$ polymorphs, δ-MnO$_2$ with edge-shared MO$_6$ octahedra have shown to exhibit decent electrochemical performances, making it a promising electrode material for electrochemical supercapacitors;[10,12,13] this is due to the fact that this polymorph is a two-dimensional layer-structured material with a relatively large interlayer distance ($\sim$7.0 Å). Recently, many studies have focused on routes and techniques for the preparation of δ-MnO$_2$. For example, Li *et al.* reported that δ-MnO$_2$ synthesized by a microwave-hydrothermal method under low pressure exhibited a specific capacitance of 210 F g^{-1} at a current density of 200 mA g^{-1} in a 1.0 M Na$_2$SO$_4$ electrolyte.[14] Ji *et al.* deposited hierarchical δ-MnO$_2$ nano-sheets directly onto a nickel foam substrate using a one-pot chelation-mediated aqueous method, and the as-prepared material exhibited a relatively high capacitance of 325 F g^{-1} at a current density of 1 A g^{-1}.[15] Zhang *et al.* synthesized δ-MnO$_2$/holey graphene hybrid fibre by activating graphene fibre in a H$_3$PO$_4$ solution, followed by the deposition of δ-MnO$_2$ on its surface.[16] The electrochemical results showed that the obtained material

[a]School of Chemical Engineering and Light Industry, Guangdong University of Technology, Guangzhou 510006, China. E-mail: jissshan@126.com

[b]Institute of Chemical Engineering, Qingdao University of Science and Technology, Qingdao, 266042, China

[c]College of Biological, Chemical Science and Chemical Engineering, Jiaxing University, Jiaxing, 314001, China

exhibited a large specific capacitance of 245 F g^{-1} at a current density of 1 A g^{-1} in a 1 M Na$_2$SO$_4$ solution. Although many efforts have been devoted to the preparation of δ-MnO$_2$ material for electrochemical supercapacitors, it still remains a challenge to obtain δ-MnO$_2$ with good cycling capability and stability. This is because (a) these 2D layered nano-structures often result in low electronic properties due to the poor contacts between each other and (b) their crystal structures are not stable under the electrochemical reactions.[17,18]

In order to improve the cycling stability and achieve better electrochemical performance of δ-MnO$_2$, an alternative and promising way is to develop hierarchical structures using different types of metal oxides. One-dimensional (1D) MnO$_2$ nano-sized materials can provide reliable electrical contact between the 1D nano-sized MnO$_2$ particles due to the formation of the three-dimensional (3D) network.[17] A hierarchical structure combining a 1D β-MnO$_2$ with a 2D δ-MnO$_2$ could result in better electrochemical performances due to (a) the good electrical conductivity of the 1D structure and, (b) the high surface area for ion adsorption on the 2D architecture improving the diffusion of the charge carriers. Also, there are many rooms in such hierarchical structure which can effectively buffer any volume change during intercalation/deintercalation of cations.[19]

In this study, the authors present a facile and low-cost approach for producing hierarchical core–shell structured mixed phase manganese oxides, consisting of β-MnO$_2$ nano-wires acting as the core to form 3D networks and δ-MnO$_2$ covered on its surface as the shell. In this investigation, the authors had for objective to produce a particle architecture that combines layered structure δ-MnO$_2$ supported on β-MnO$_2$ nano-wires. Through this unusual structural design, the obtained core–shell structured manganese oxide exhibited both high cycling stability and high electrochemical performance.

2. Experimental

2.1 Preparation of the samples

All reagents were of analytic grade (AR) and double-distilled water was used all throughout the experiments. To prepare the 1D β-MnO$_2$ nano-wires, 8 mmol of MnSO$_4$ and 8 mmol of (NH$_4$)$_2$SO$_4$ were added to 60 mL H$_2$O under intense stirring (magnetic stirrer). Then this solution was transferred to a 100 mL Teflon-lined stainless-steel autoclave and heated at 120 °C for 12 h. The autoclave was cooled to room temperature, and the product was filtered, washed with water and dried at 80 °C for 12 h. The resultant material was made of 1D β-MnO$_2$ nano-wires.

To prepare β-MnO$_2$@δ-MnO$_2$, 60 mg of the as-prepared 1D β-MnO$_2$ nano-wires was added to 30 mL of 0.41 mmol MnSO$_4$ solution and ultrasonicated for 10 min using an ultrasonic bath operating at 40 kHz. The obtained mixture was dropwise added to 20 mL of 0.28 KMnO$_4$ solution and then kept at room temperature for 30 min. Then the product was collected (centrifuge), filtered, washed with water, and finally dried at 80 °C for 12 h. The obtained product was made of β-MnO$_2$@δ-MnO$_2$.

For comparison purposes, pure δ-MnO$_2$ was also prepared and the detail procedure is as follows: 30 mL of 0.41 mmol MnSO$_4$ was dropwise added to 20 mL of 0.28 KMnO$_4$ solution. The reaction was further allowed to proceed at room temperature for 30 min. The obtained pure δ-MnO$_2$ was filtered, washed with water and dried at 80 °C for 12 h.

2.2 Physical characterizations

XRD patterns were recorded on a Shimadzu XD-3A (Japan) using filtered Cu-Kα radiation (λ = 0.15418 nm) generated at 40 kV and at 30 mA. Scans for 2θ values were recorded at 4° min^{-1}. Scanning electron microscopy (SEM) images were obtained using a Carl Zeiss Ultra Plus. Transmission electron microscopy (TEM) high angle annular dark field scanning transmission electron microscopy (STEM) images and selected area electron diffraction (SAED) patterns of the catalysts were obtained using a JEOL (JEM-2000 FX) microscope operating at 200 kV. Line-scan energy dispersive spectroscopy (EDS) in the STEM mode was used for elemental composition analysis. The sorption isotherms were obtained on a Quantachrome Autosorb-1 volumetric analyzer. Specific surface areas were determined by the Brunauer–Emmett–Teller (BET) method.

2.3 Electrochemical characterizations

Cyclic voltammograms (CV) and galvanostatic charge/discharge experiments on the as-prepared materials were carried out in a three-electrode electrochemical cell. The working electrode (WE) consisted of a film (1 cm^2) containing β-MnO$_2$@δ-MnO$_2$ (10 mg), carbon black and poly(tetrafluoroethylene) with a mass ratio of 80 : 10 : 10, pressed into the Ni foam current collectors. An Hg/HgO (1.0 M KOH) reference electrode (REF) and an activated carbon counter electrode (CE) was used in all experiments in 1 mol L^{-1} LiOH electrolyte. CV experiments were performed on a CHI 650D electrochemical workstation. Galvanostatic charge/discharge tests were carried out on a Neware Battery Tester (BTS6.0, Neware Technology Company, Guangdong, China).

3. Results and discussion

Fig. 1 shows the powder X-ray diffraction (XRD) patterns of β-MnO$_2$, δ-MnO$_2$ and β-MnO$_2$@δ-MnO$_2$. The XRD pattern of β-MnO$_2$ shows the typical peak dispersion indexed to β-MnO$_2$ tetragonal phase (Joint Committee on Powder Diffraction Standards [JCPDS] Card 24-0735), in which no peaks related to other types of MnO$_2$ or amorphous MnO$_2$ are observed, indicative of the formation of highly pure and crystalline β-MnO$_2$. The diffraction peaks of δ-MnO$_2$, synthesized at room temperature, are exhibited at angles of 37.2° and 67.2° which are ascribed to (111) and (021) planes of δ-MnO$_2$ (JCPDS Card: 42-1317) respectively. However, these peaks are small and weak, indicating that the as-prepared δ-MnO$_2$ particles are small and poorly crystalline. Similar XRD patterns of δ-MnO$_2$ were also found in the literature where the δ-MnO$_2$ samples were prepared at low temperature.[15,20,21] In the case of β-MnO$_2$@δ-MnO$_2$, its XRD pattern shows no obvious difference from β-
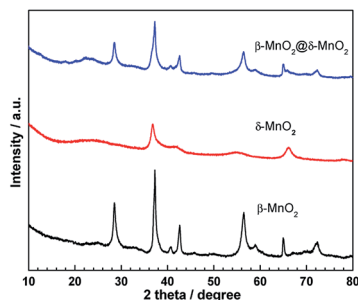
Fig. 1 XRD patterns of β-MnO$_2$, δ-MnO$_2$ and β-MnO$_2$@δ-MnO$_2$.

MnO$_2$, for example the peaks resemble to those associated to a β-MnO$_2$ structure indicating that a small amount of δ-MnO$_2$ was formed on the surface of β-MnO$_2$.

Scanning electron microscope (SEM) and transmission electron microscope (TEM) images of β-MnO$_2$ and β-MnO$_2$@δ-MnO$_2$ are shown in Fig. 2(A). shows that the as-prepared β-MnO$_2$ particles are needle-like in shape and have a size of *ca.* 2–5 μm in length by direct statistic observation. The figure also shows that there is no presence of other forms of particles, indicating that highly pure β-MnO$_2$ with uniform morphology was formed, which is in very good agreement with the XRD results. SEM image of δ-MnO$_2$ is shown in Fig. 2(C), which comprise irregular particles and many particles aggregated into large particles. As shown in Fig. 2(B), a uniform hierarchical β-MnO$_2$@δ-MnO$_2$ core–shell structure was formed after the δ-MnO$_2$ was deposited on the surface of β-MnO$_2$ *via* the simple

wet chemistry method at room temperature. From the figure, it can be seen that the δ-MnO$_2$ is hardly formed in the spaces between the β-MnO$_2$ nano-wires, implying that the formation of δ-MnO$_2$ preferentially occurs on the surface of β-MnO$_2$ nano-wires resulting in an uniform β-MnO$_2$@δ-MnO$_2$ core–shell structure. Fig. 2(E) shows a typical TEM image of β-MnO$_2$@δ-MnO$_2$. The figure shows that the β-MnO$_2$ has a uniform nano-wire structure with a diameter of *ca.* 70 nm. It can also be seen that δ-MnO$_2$ was uniformly distributed on the surface of β-MnO$_2$ nano-wires with a thickness of *ca.* 30 nm. However, there is no obvious evidence of boundaries between the β-MnO$_2$ core and δ-MnO$_2$ shell, showing that an intimate contact between these two different phases of MnO$_2$ exists. On the edge of the δ-MnO$_2$ shell, ultra-thin δ-MnO$_2$ nano-sheets are found and expected to provide improved electrochemical properties. Fig. 2(F) shows a detailed microstructure of the core and shell of β-MnO$_2$@δ-MnO$_2$, in which the atomic plane arrangement of β-MnO$_2$ is clearly present, but with the absence of an atomic plane in the shell of δ-MnO$_2$. This finding further confirms that the δ-MnO$_2$ grown on the surface of β-MnO$_2$ is small and is of a poor crystalline structure. It is also observed that the δ-MnO$_2$ shell with layered structure was formed on the surface of β-MnO$_2$ nano-wires. Such a layered structure is expected to facilitate the intercalation/deintercalation of cations into and from the electrode materials resulting in an improved electrochemical capacitance performance.

The porous structures of β-MnO$_2$, δ-MnO$_2$ and β-MnO$_2$@δ-MnO$_2$ were evaluated by N$_2$ isotherm analysis (Fig. 3 and Table 1). The nitrogen adsorption–desorption isotherms of β-MnO$_2$, shows a type II isotherm (as defined by the International Union of Pure and Applied Chemistry (IUPAC)) with a sharp capillary condensation step at a relative high pressure ($P/P_0 >$ 0.85). An hysteresis loop between adsorption and desorption curve could be considered as an H4-type, indicating a relatively large pore size, which could be due to the slit-shaped gap among the MnO$_2$ crystals.[22] The isotherm of β-MnO$_2$@δ-MnO$_2$ also exhibits type II with a hysteresis loop at a high relative pressure, indicating that the as-prepared material is of a meso-porous nature. The isotherms of δ-MnO$_2$ is a mixed type in the IUPAC classification with a type I at a relative low pressure and a type II with an hysteresis loop at a relative intermediate and high pressure.[23] At the initial part, there is an obvious uptake at a low relative pressure, which is a characteristic of a micropo-rous structure. As shown in Fig. 3(B), the pore size distributions calculated from the Barrett–Joyner–Halenda (BJH) method show that the pore size distributions of δ-MnO$_2$ and β-MnO$_2$@δ-
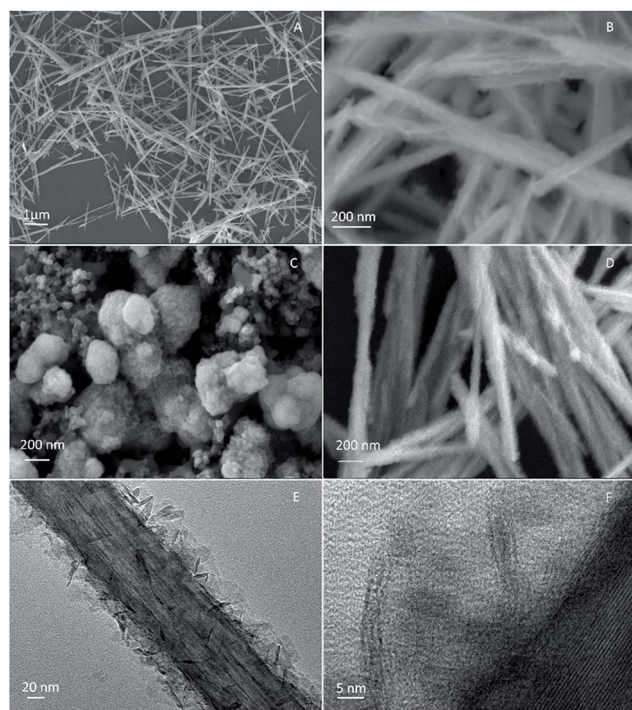

Fig. 2 SEM images of β-MnO$_2$ (A), β-MnO$_2$@δ-MnO$_2$ (B), δ-MnO$_2$ (C) and β-MnO$_2$@δ-MnO$_2$ after 5000 cycles (D), TEM image of β-MnO$_2$@δ-MnO$_2$ (E) and HRTEM image of β-MnO$_2$@δ-MnO$_2$ (F).
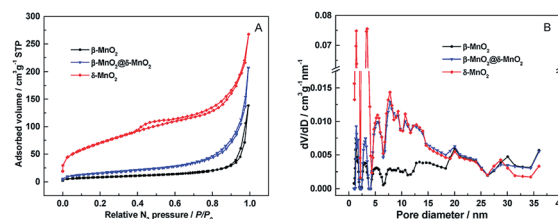

Fig. 3 N$_2$ isotherms (A) and pore size distribution (B) of β-MnO$_2$, δ-MnO$_2$ and β-MnO$_2$@δ-MnO$_2$.

Table 1 Porous structure of β-MnO₂, δ-MnO₂ and β-MnO₂@δ-MnO₂

Samples	BET ($m^2\ g^{-1}$)	Pore volume ($cm^3\ g^{-1}$)
β-MnO₂	30.06	0.214
β-MnO₂@δ-MnO₂	56.44	0.321
δ-MnO₂	248.91	0.414

MnO₂ are in the mesopore size range with a few micropores present. The BET surface area of δ-MnO₂ was found to be 248.91 $m^2\ g^{-1}$, which is ~8 times higher than that of 1D β-MnO₂ (30.06 $m^2\ g^{-1}$). After δ-MnO₂ was grown on the surface of needle-like 1D β-MnO₂, the BET surface area of β-MnO₂@δ-MnO₂ was determined to be 56.44 $m^2\ g^{-1}$, which is almost twice as high as that of β-MnO₂, but still much lower than that of δ-MnO₂, due to the presence of a thin layer of δ-MnO₂ grown on β-MnO₂.

The electrochemical performance of the as-prepared β-MnO₂, δ-MnO₂ and β-MnO₂@δ-MnO₂ was evaluated by cyclic voltammetry (CV) and galvanostatic charge–discharge experiments in a three-electrode cell configuration and in 1 mol L^{-1} LiOH electrolyte. Fig. 4(A) shows the CVs of the β-MnO₂, δ-MnO₂ and β-MnO₂@δ-MnO₂ electrodes at a scan rate of 5 mV s^{-1} in 1.0 M LiOH solution and at room temperature. The figure shows that the CVs for the three samples exhibit a quasi-rectangular shape, typical of a pseudo-capacitive behaviour, with pairs of redox peaks corresponding to the reversible Faradaic redox reactions. The charge storage of MnO₂-based electrodes results from the adsorption/desorption and the intercalation/ deintercalation of cations or protons of the electrolyte.[11] The morphology, crystal structure and surface area play an important role in storing the charges. The current response on δ-MnO₂ is the highest among these three electrodes, suggesting that the high surface area and the layered structure favour the intercalation/deintercalation process as well as the adsorption/ desorption occurring on the surface. On the β-MnO₂@δ-MnO₂

electrode, the current response is higher than that of the β-MnO₂ electrode, indicating additional capacitive contribution from δ-MnO₂ after it had been deposited on the surface of β-MnO₂. Fig. 4(C) and (D) show the CVs of β-MnO₂, δ-MnO₂ and β-MnO₂@δ-MnO₂ electrodes carried out over the potential range of −0.15 to +0.60 V *vs.* Hg/HgO at various scan rates (5–100 mV s^{-1}). When the scan rate increases from 5 to 100 mV s^{-1}, the CVs of β-MnO₂ still retain a quasi-rectangular shape, even though the Faradaic process revolves around the electrochemical behaviour of β-MnO₂ in 1 M LiOH electrolyte, implying that the adsorption/desorption process dominates the charge storage process in β-MnO₂. In the case of δ-MnO₂ and β-MnO₂@δ-MnO₂, due to the layered structure of β-MnO₂, the Faradaic process contributed proportionally more to the charge storage than the electrical double-layer capacitance. Therefore, with increasing the scan rate, the CVs of δ-MnO₂ and β-MnO₂@δ-MnO₂ exhibit a distortion/change from quasi-rectangular shape due to electrode polarization. At fast scan rates, there is barely time for some Li⁺ ions to intercalate into the MnO₂ structure due to the polarization of the desolvation process of Li⁺ ions, resulting in the CVs deviating from the quasi-rectangular shape.[24]

Fig. 5 shows the galvanostatic charge–discharge curves of the β-MnO₂, δ-MnO₂ and β-MnO₂@δ-MnO₂ at a current density of 50 mA g^{-1}. All three electrodes present non-linear charge curves, asymmetric to their corresponding discharge curves (as shown in Fig. 5(A)), which is commonly and typically observed for pseudo-capacitive materials.[25] The charge–discharge curves exhibit a quasi-plateau over the potential range from +0.3 to +0.5 V *vs.* Hg/HgO. This quasi-plateau could originate from the intercalation/deintercalation of Li⁺ into or from MnO₂ structure which is consistent with the CV curves. The specific capacitance (C_s) values derived from the discharge curves were calculated using the following equation:

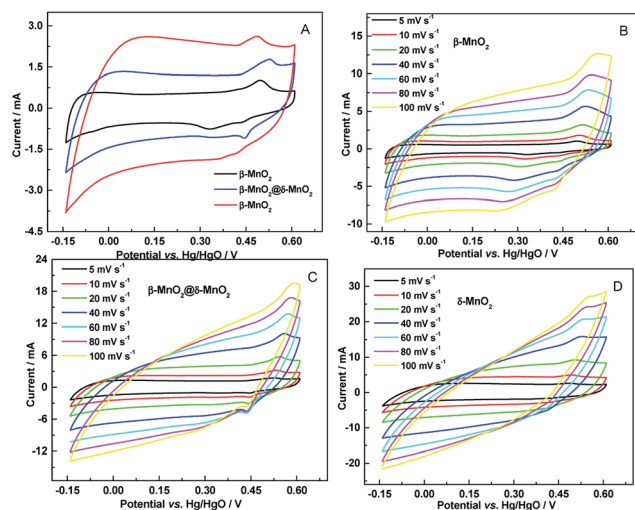$$c(F/g) = \frac{I\Delta t}{m\Delta V} \qquad (1)$$

Fig. 4 (A) CVs of β-MnO₂, δ-MnO₂ and β-MnO₂@δ-MnO₂ electrodes at scan rate of 5 mV s^{-1} and (B–D) their corresponding CVs at various scan rates (5–100 mV s^{-1}) in 1 M LiOH.
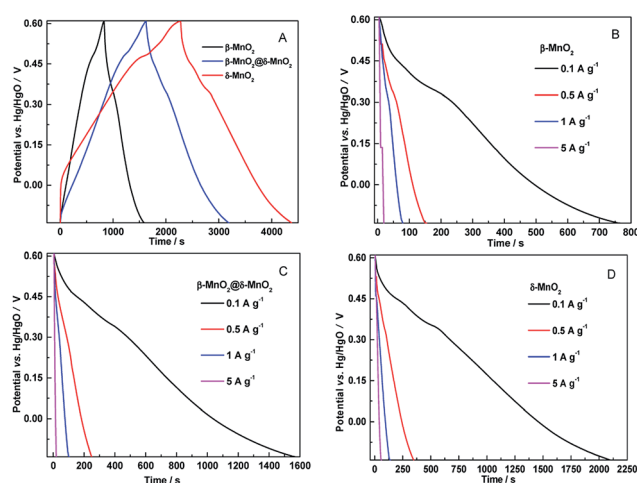

Fig. 5 Galvanostatic charge–discharge curves of the β-MnO₂, δ-MnO₂ and β-MnO₂@δ-MnO₂ at a current density of 50 mA g^{-1} (A), discharge curves of β-MnO₂ (B), β-MnO₂@δ-MnO₂ (C) and δ-MnO₂ (D) electrodes at various current densities.

where I is the sampled current, t is the sampling time span, V is the total potential deviation of the potential window, and m is the mass of the active electrode material. C_s discharge values of β-MnO_2, δ-MnO_2 and β-MnO_2@δ-MnO_2 were found to be 100.3, 246.9 and 200.8 F g^{-1} respectively. The increase in C_s from the β-MnO_2 to δ-MnO_2 indicates that the layered structure δ-MnO_2 with high surface area contributed to C_s in correlation with the CV results. Rate capability testing of β-MnO_2, δ-MnO_2 and β-MnO_2@δ-MnO_2 was evaluated at current densities ranging from 0.1 A g^{-1} to 5 A g^{-1} and the data are shown in Fig. 5(C and D). The results of rate capability experiments show that the specific capacitance decreased with increased current density, which is in good agreement with reported literature on MnO_2-based electrodes.[4,26,27] When the current density increases from beyond 0.5 A g^{-1}, the quasi-plateau gradually disappears owing to the incomplete intercalation/deintercalation process.

The effect of the current density on the specific capacitance of β-MnO_2, δ-MnO_2 and β-MnO_2@δ-MnO_2 is shown in Fig. 6. It is clearly evident from the figure that the C_s for all three samples gradually decreased when the current densities increased from 0.05 to 5 A g^{-1}. At the low current densities, all three electrodes show relatively high capacitance since the electrolyte ions have enough time to move to the interface of the electrode/electrolyte and take part to the intercalation/deintercalation process. At a current density of 5 A g^{-1}, only a small portion of the material close to the surface can be utilized for storing the charge. The C_s of β-MnO_2, δ-MnO_2 and β-MnO_2@δ-MnO_2 at a current density of 5 A g^{-1} retain 38.4, 34.8 and 37.2 of their initial values at a current density of 0.1 A g^{-1}, indicating that these three electrodes have similar rate capabilities.

Cycling stability is another critical requirement for high-performance supercapacitor. The cycling life tests for β-MnO_2, δ-MnO_2 and β-MnO_2@δ-MnO_2 were measured over 5000 continuous charge–discharge cycles between -0.15 to $+0.6$ V $vs.$ Hg/HgO at a current density of 1 A g^{-1} as shown in Fig. 7.

In the case of δ-MnO_2, the C_s gradually decreases with increasing cycling numbers. After 5000 cycles, $ca.$ 75% of its initial capacitance is retained. Compared to δ-MnO_2, β-MnO_2 and β-MnO_2@δ-MnO_2 show excellent cycling stability. After 5000 cycles, the specific capacitance retention of β-MnO_2@δ-MnO_2 is almost unchanged, and the coulombic efficiency of β-MnO_2 is almost 100% (98.9%) as shown in Fig. 8, suggesting

Fig. 7 Cycling stability of β-MnO_2, δ-MnO_2 and β-MnO_2@δ-MnO_2 at a current density of 1 A g^{-1} in 1 M LiOH electrolyte.

that the 1D β-MnO_2 pocesses superior cycling stability and the hierarchical core–shell structured β-MnO_2@δ-MnO_2 using 1D β-MnO_2 as backbones, retain the cycling stability of the 1D β-MnO_2. The stability of β-MnO_2@δ-MnO_2 is also much greater than that of other reported MnO_2-based electrode materials, such as $NiCo_2O_4$-doped carbon nanofiber@MnO_2 core–sheath nanostructures,[28] mesoporous MnO_2/carbon aerogel composite,[29] δ-MnO_2 nanospheres[14] and MnO_2 core–shell nanowires.[30] In terms of charge storage mechanism in MnO_2-based electrodes,[24] the charge storage process is based upon the adsorption/desorption of electrolyte ions, accompanied by redox conversion between Mn^{4+} and Mn^{3+}. Based on this mechanism, the excellent cyclability of β-MnO_2@δ-MnO_2 could be attributed to the fact that the Faradic redox process occurred near the electrode surface, which in turns may not possibly cause serious modification in the crystal structure and morphology of the electrode material. The cycling stability testing causes negligible damage on the structure of β-MnO_2@δ-MnO_2, resulting in the excellent cycling stability. Although the surfaces of both β-MnO_2@δ-MnO_2 and δ-MnO_2

Fig. 6 Specific capacitance of β-MnO_2, δ-MnO_2 and β-MnO_2@δ-MnO_2 at different current densities in 1 M LiOH electrolyte.
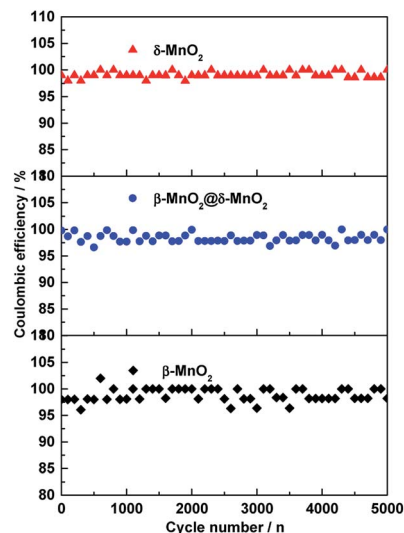
Fig. 8 Coulombic efficiency of β-MnO_2, δ-MnO_2 and β-MnO_2@δ-MnO_2 electrodes for 5000 cycles at a current density of 1 A g^{-1}.

were covered by layered structure δ-MnO₂, β-MnO₂@δ-MnO₂ exhibits much better stability than δ-MnO₂ since 1D β-MnO₂ can serve as a stable structural supportive backbone, which could reduce the structural damage during the reversible Faradaic redox reactions occurring in MnO₂. Meanwhile, synergistic effects between core–shell structured manganese oxides with different structures and dimensions could be another reason resulting in the improved cycling stability. The excellent cyclability of β-MnO₂@δ-MnO₂ of the core–shell structure offers a promising target structure for future research.

The Nyquist plots of the electrochemical impedance spectroscopy (EIS) of β-MnO₂, δ-MnO₂ and β-MnO₂@δ-MnO₂ electrodes are present in Fig. 9(A). All plots show semicircles at the higher frequency region and straight lines at the lower frequency region. The diameters of the semicircles in the high-frequency represent the Faradic charge transfer resistance of the redox reactions at the electrode–electrolyte interface. It can be observed from Fig. 9(A) that the charge transfer resistance of β-MnO₂@δ-MnO₂ is lower than that of β-MnO₂ and δ-MnO₂, suggesting that the charge transfer is the fastest one among these three samples. The straight lines on the EIS spectra correspond to the ion diffusion process in the bulk of the active mass in the low-frequency region. The slope (of the straight line) of β-MnO₂ is larger than that of β-MnO₂@δ-MnO₂ and δ-MnO₂, indicating that the ion diffusion resistance on β-MnO₂ is the smallest among the three samples. The slope of β-MnO₂@δ-MnO₂ is slightly higher than that of δ-MnO₂, suggesting that β-MnO₂ can provide faster ion diffusion in the bulk of the active mass and faster Faradic charge transfer on the interface of electrode–electrolyte when core–shell structured β-MnO₂@δ-MnO₂ is formed. Fig. 9(B) shows the EIS curves of β-MnO₂@δ-MnO₂ before and after 5000 cycles. It can be observed that semicircles at the higher frequency region are quite similar, indicating, after 5000 cycles, the charge transfer resistance of β-MnO₂@δ-MnO₂ almost didn't change. The slope of β-MnO₂@δ-MnO₂ is slightly smaller than that of β-MnO₂@δ-MnO₂ after 5000 cycles, suggesting that the ion diffusion resistance on β-MnO₂@δ-MnO₂ after 5000 cycles only increase a little bit. The EIS results clearly show that the structure of β-MnO₂@δ-MnO₂ is very stable in 1 M LiOH electrolyte. The SEM image of β-MnO₂@δ-MnO₂ after 5000 cycles (shown in Fig. 2(D)) also confirms its structural stability.
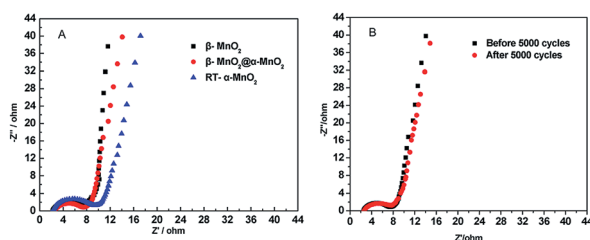

Fig. 9 (A) Electrochemical impedance spectroscopy (EIS) curves of β-MnO₂, δ-MnO₂ and β-MnO₂@δ-MnO₂; (B) EIS curves of β-MnO₂@δ-MnO₂ before and after 5000 cycles.

4. Conclusions

In summary, a hierarchical β-MnO₂@δ-MnO₂ core–shell structure with β-MnO₂ nano-wires as cores and layered structure δ-MnO₂ as shells were synthesized via a simple wet chemical method. Compared to δ-MnO₂ and β-MnO₂, β-MnO₂@δ-MnO₂ shows excellent cycling stability. The capacitance retention of β-MnO₂@δ-MnO₂ is almost unchanged with coulombic efficiency values close to 100% after 5000 cycles. It was found that the excellent cycling stability of β-MnO₂@δ-MnO₂ arises from synergistic effects between the core–shell structured manganese oxides with different structures/dimensions and the 1D β-MnO₂ used as a stable structural supportive backbone, which could reduce the structural damage during the reversible Faradaic redox reactions occurring in MnO₂. Therefore the as-prepared β-MnO₂@δ-MnO₂ offers a new promising cathode candidate material for alkali supercapacitors.

Acknowledgements

References

1 A. Gambou-Bosca and D. Bélanger, *Electrochim. Acta*, 2016, **201**, 20–29.
2 T. Wang, F. Dong and Y. X. Zhang, *Mater. Lett.*, 2016, **171**, 319–322.
3 G. He, M. Qiao, W. Li, Y. Lu, T. Zhao, R. Zou, B. Li, J. A. Darr, J. Hu, M.-M. Titirici and I. P. Parkin, *Adv. Sci.*, 2017, **4**, 1600214.
4 M. Huang, F. Li, F. Dong, Y. X. Zhang and L. L. Zhang, *J. Mater. Chem. A*, 2015, **3**, 21380–21423.
5 S. J. Zhu, J. Q. Jia, T. Wang, D. Zhao, J. Yang, F. Dong, Z. G. Shang and Y. X. Zhang, *Chem. Commun.*, 2015, **51**, 14840–14843.
6 J. Shao, X. Zhou, Q. Liu, R. Zou, W. Li, J. Yang and J. Hu, *J. Mater. Chem. A*, 2015, **3**, 6168–6176.
7 W. Li, J. Wang, G. He, L. Yu, N. Noor, Y. Sun, X. Zhou, J. Hu and I. P. Parkin, *J. Mater. Chem. A*, 2017, **5**, 4352–4358.
8 Z.-S. Wu, W. Ren, D.-W. Wang, F. Li, B. Liu and H.-M. Cheng, *ACS Nano*, 2010, **4**, 5835–5842.
9 M. H. Alfaruqi, J. Gim, S. Kim, J. Song, D. T. Pham, J. Jo, Z. Xiu, V. Mathew and J. Kim, *Electrochem. Commun.*, 2015, **60**, 121–125.
10 S. Devaraj and N. Munichandraiah, *J. Phys. Chem. C*, 2008, **112**, 4406–4417.
11 S. Bag and C. R. Raj, *J. Mater. Chem. A*, 2016, **4**, 8384–8394.
12 A. M. Kannan, S. Bhavaraju, F. Prado, M. M. Raja and A. Manthiram, *J. Electrochem. Soc.*, 2002, **149**, A483–A492.
13 J. Cao, Q. Mao, L. Shi and Y. Qian, *J. Mater. Chem.*, 2011, **21**, 16210.
14 B. Ming, J. Li, F. Kang, G. Pang, Y. Zhang, L. Chen, J. Xu and X. Wang, *J. Power Sources*, 2012, **198**, 428–431.

15 M. Pang, G. Long, S. Jiang, Y. Ji, W. Han, B. Wang, X. Liu and Y. Xi, *Electrochim. Acta*, 2015, **161**, 297–304.

16 J. Zhang, X. Yang, Y. He, Y. Bai, L. Kang, H. Xu, F. Shi, Z. Lei and Z.-H. Liu, *J. Mater. Chem. A*, 2016, **4**, 9088–9096.

17 J. Zhu, W. Shi, N. Xiao, X. Rui, H. Tan, X. Lu, H. H. Hng, J. Ma and Q. Yan, *ACS Appl. Mater. Interfaces*, 2012, **4**, 2769–2774.

18 T. T. Truong, Y. Liu, Y. Ren, L. Trahey and Y. Sun, *ACS Nano*, 2012, **6**, 8067–8077.

19 S. W. Lee, B. M. Gallant, H. R. Byon, P. T. Hammond and Y. Shao-Horn, *Energy Environ. Sci.*, 2011, **4**, 1972–1985.

20 G. Zhu, H. Li, L. Deng and Z.-H. Liu, *Mater. Lett.*, 2010, **64**, 1763–1765.

21 X. Zhang, X. Chang, N. Chen, K. Wang, L. Kang and Z.-h. Liu, *J. Mater. Sci.*, 2012, **47**, 999–1003.

22 Z. Jia, J. Wang, Y. Wang, B. Li, B. Wang, T. Qi and X. Wang, *J. Mater. Sci. Technol.*, 2016, **32**, 147–152.

23 S. Brunauer, L. S. Deming, W. E. Deming and E. Teller, *J. Am. Chem. Soc.*, 1940, **62**, 1723–1733.

24 Q. Qu, P. Zhang, B. Wang, Y. Chen, S. Tian, Y. Wu and R. Holze, *J. Phys. Chem. C*, 2009, **113**, 14020–14027.

25 K. Wang, C. Zhao, S. Min and X. Qian, *Electrochim. Acta*, 2015, **165**, 314–322.

26 Y. Hu, J. Wang, X. Jiang, Y. Zheng and Z. Chen, *Appl. Surf. Sci.*, 2013, **271**, 193–201.

27 J. An, X. Peng, S. Xu, Z. Xu and J. Wang, *RSC Adv.*, 2015, **5**, 97080–97088.

28 F. Lai, Y.-E. Miao, Y. Huang, T.-S. Chung and T. Liu, *J. Phys. Chem. C*, 2015, **119**, 13442–13450.

29 G.-R. Li, Z.-P. Feng, Y.-N. Ou, D. Wu, R. Fu and Y.-X. Tong, *Langmuir*, 2010, **26**, 2209–2213.

30 X. Zhang, J. Ma, W. Yang, Z. Gao, J. Wang, Q. Liu, J. Liu and X. Jing, *CrystEngComm*, 2014, **16**, 4016.